JNTM JOURNAL of NEW TECHNOLOGY and MATERIALS

Journal of New Technology and Materials

Vol. 15, No. 1 (2025), 46–60

RESEARCH ARTICLE

Delay-Resolved Elastochemical Susceptibility Mapping of Communication-Induced Oscillations in Responsive Hydrogel Colloid Monolayers

T. Layne[1,*] and W. Kim[2]

[1]Department of Materials Science and Engineering, Yonsei University, 50 Yonsei-ro, Seodaemun-gu, Seoul 03722, Republic of Korea. [2]Materials Research Laboratory and Materials Science Department, University of Illinois, 104 South Goodwin, Urbana, Illinois 61801

*Correspondence: layne29@@yonsei.ac.kr

Received date: Janaury 11, 2025; Accepted date: May 18, 2025

Abstract

Chemically communicating hydrogel colloids provide a responsive soft-material system in which chemical transformation, diffusive signaling, particle-volume variation, and elastic packing are tightly coupled processes. The materials challenge that remains to be resolved is how a monostable colloid, without needing a chemical clock within each individual particle, enters oscillatory or wave states after being embedded in a communicating layer. The present work enhances that challenge by introducing a delay-resolved elastochemical susceptibility approach to the two-dimensional assembly of hydrogels. The approach employs the normalized density range $\rho\sigma_0^2 \approx 0.01$–$3.0$, the communication coordinate $\widehat{m} = m/(q\sigma_0/c_c) \approx 0$–$20$, the instantaneous diameter σ_i, the internal proton concentration c_i, the Yukawa neighbour field Y_{ji}, the Hertzian contact, and Brownian dynamics to differentiate chemical stimulation from packing interactions. In particular, the lagged correlation between previously encountered and currently experienced chemical fields provides the primary test for chemical stimulation. A negative delayed susceptibility implies that shrinkage follows chemical exposure; the evaluation of communication strength, antiphase scoring, spectral neighbor depth, and finite wavenumber/frequency reveals whether the localized delayed susceptibility generates a dynamic fluctuation regime, an antiphase shell limit state, a propagating cluster wave, or a mechanically trapped active solid. The conclusion drawn from this analysis is that communication alone is insufficient to generate oscillations: all four conditions need to be met simultaneously. It thus becomes clear that the density–communication phase diagram must be interpreted differently, as a design parameter for soft colloidal materials in which the collective response arises endogenously from chemical and mechanical coupling.

Keywords: responsive hydrogel colloids, active soft matter, chemical communication, chemo-mechanical coupling, Brownian dynamics, delay susceptibility, cluster waves, new technology materials

1 Introduction

The increasing focus on responsive soft systems as materials in which sensing, actuation, and spatial organization emerge from coupled physicochemical properties is complemented by new research on hydrogel colloids. The polymer network of a hydrogel colloid serves as the structural component responsible not only for elasticity but also for solvent uptake and molecular permeability, thus directly relating volume change to chemical properties. For example, swelling in a hydrogel particle increases the volume available for solute access, while collapsing decreases permeability and free volume. This coupling of chemical conversion to physical deformations allows chemical changes to influence mechanics and vice versa. In other words, the hydrogel system is characterized by a complex feedback relationship between chemical fields and deformations in which chemical signal processing translates into mechanical reorganization. In contrast to simple suspensions of inert soft particles, the material is thus highly organized with respect to chemical and elastic degrees of freedom that are coupled to each other to form spatiotemporal patterns.

Chemical signal-processing systems that influence the mechanical organization of matter are found in living systems in the form of quorum sensing, developmental patterning, and morphogen formation [1–3]. The chemical systems employed by synthetic materials lack the regulation found in cells but allow the integration of chemical reaction, molecular diffusion, and mechanical deformation into one material unit [4–6]. Recent work on collectively responsive hydrogels has shown that oscillations can occur in an assembly of gel particles below the threshold for self-oscillation, making it possible to decrease the autonomy required for collective response by relying on communication and crowding in lieu of independent local clocks [7]. This is critical for material design since the focus of interest should shift from bistability of individual units to crowd-induced communication.

Chemically coupled active matter represents a related literature tradition that has been shown to lead to self-organization in phoretic particles, chemotactic particles, chemically coupled microswimmers, and chemically interacting particles that self-assemble into clusters and aster patterns, migrate as domains, and segregate into nonequilibrium phases [8–10]. The above work emphasizes the capacity of chemical fields to communicate between agents but largely explains the observed phenomena in terms of mobility and directed motion. Active but non-motile hydrogel colloids call for an entirely different description since the main feature of their activity is neither motility nor directional self-propulsion. Rather, activity manifests as a change in particle diameter and elasticity, while the particles themselves continue moving Brownianly. In this context, an important question concerns whether communication can result in the prediction of future particle deformations, which in turn will induce mechanical reorganization of neighbouring particles.

It is especially important for this problem to consider recent theoretical models of communication in micro- and nanoparticles that highlight the necessity of incorporating multiple aspects of the communication process into simulations, namely molecular generation and consumption rates, diffusion length, signal lifetime, receptor or response kinetics, and packing [11]. All these aspects become even more important for hydrogel colloids where chemical processes and mechanical deformation are linked via the polymer network of the particle. Permeability sets the rate of molecular production or loss, and molecules determine the degree of swelling and hence the diameter of the particle. Chemical interaction then changes the contact distance and the amplitude of the cloud around the particle. Microreactor models have demonstrated that by controlling permeability, signal lifetime, and volume sensitivity of the chemical reaction, it is possible to set up different regimes ranging from monostable to oscillatory [12]. The present paper seeks to extend this reasoning to many-particle systems in the hope that a set of many-particle descriptors may distinguish between chemical and static influences on the system.

The model most relevant for simulations of hydrogel-colloid systems was developed by Göth and Dzubiella [13], in which chemically reactive, but not motile, size-responsive hydrogel particles are simulated as Brownian particles interacting via a contact interaction, diameter potential, diffusion of molecules in a Yukawa field, and proton generation and loss. This model showed that monostable particles exhibit collective antiphase oscillations and cluster waves under appropriate conditions of density and communication. It also showed that these conditions cannot always be captured simply by considering the density versus signal strength parameter space since the latter does not provide information about the nature of crowding: the same parameters can represent chemically inactive but mechanically packed particles, chemically active but dilute particles that do not interact enough to experience mutual communication, and chemically active and dense particles. The important conclusion is thus that one must account for the temporal succession of events in the chemical–mechanical cascade by identifying whether the chemical signal sensed by the particle at a certain time t results in the particle diameter change at $t + \Delta$ and subsequent mechanical reorganization.

The situation with hydrogel colloids is even more complicated by the fact that density can mean different things depending on the context. Nominal density defined in terms of the average particle diameter is quite distinct from actual particle packing, and communication may change the packing state significantly even when the nominal density remains relatively high. On the contrary, small nominal densities and strong communication can lead to mechanically denser packing states, in which particle diameters are large. This means that the chemical state of the system and its packing properties must be assessed simultaneously in order to understand whether the particles form clusters of certain packing states or wave-like structures. Failure to distinguish between these packing states could lead to the misinterpretation of wave states as jammed and oscillatory states as weakly communicating ones.

In view of this context, the present paper introduces four novel descriptors that can help analyze the state of a system of communicating hydrogel colloids, namely the delay-resolved lagged chemical signal–particle diameter susceptibility, packing-corrected communication number, antiphase score for neighbouring particles in terms of particle diameter, and spectral cluster-wave score that considers frequency and spatial structure of wave states. The term *delay-resolved* is justified by the fact that this descriptor takes account of the delay between sensing the chemical signal and reacting to it by changing the particle size and elasticity, while *elastochemical* denotes that the particle diameter is considered along with contact mechanics, compressibility, and packing state. The paper attempts to answer the following question: under what conditions are the above characteristics satisfied in the case of a monostable responsive hydrogel colloid?

2 Methodology

The subject belongs directly to the materials-science and engineering scope of the *Journal of New Technology and Materials*. The investigated system is a chemically communicating soft material composed of responsive hydrogel colloids, and the analysis addresses how nanoscale-to-microscale colloidal architecture, polymer-network permeability, elastic deformation, and chemical signalling can be selected to produce engineered collective response. This emphasis on new material behaviour, soft-material functionality, and nanotechnology-associated colloidal design is consistent with a journal scope centred on materials science, engineering, and materials associated with new technologies.

The computational material is a quasi-two-dimensional periodic monolayer of catalytically active, non-motile, size-responsive hydrogel colloids. Each colloid is represented by two translational coordinates $\mathbf{x}_i = (x_i, y_i)$, one instantaneous diameter σ_i, and one internal proton concentration c_i. The governing quantities are the normalized density coordinate $\rho\sigma_0^2 \approx 0.01$–$3.0$, the communication coordinate $\widehat{m} = m/(q\sigma_0/c_c) \approx 0$–$20$, the communication length $\kappa^{-1} = \sigma_0$, the elastic strength $\epsilon = 500\, k_\mathrm{B}\, T$, the size stiffness $q = 100\, k_\mathrm{B}\, T/\sigma_0^2$, the size-friction coefficient $\xi_\sigma = 10\xi_x^0$, the production and loss constants $k_0 = 2.749/\tau$ and $k_l = 1/\tau$, the sieve parameter $B = \sigma_0^3$, the timestep $\Delta t = 10^{-4}\tau$, the relaxation interval 5τ, and the measurement window 40τ. These quantities follow the communicating hydrogel-colloid formulation of Göth and Dzubiella [13] and provide the numerical basis for the delay-resolved elastochemical analysis.

The simulated material geometry is illustrated in Figure 1. The blue hydrogel discs represent deformable colloids whose instantaneous diameters change with the internal chemical state, while the pale green halos denote the finite communication range over which neighbouring particles contribute to the received signal. This view links the normalized density coordinate to a physical monolayer and shows why the same particle arrangement must be read through both mechanical crowding and chemical communication.

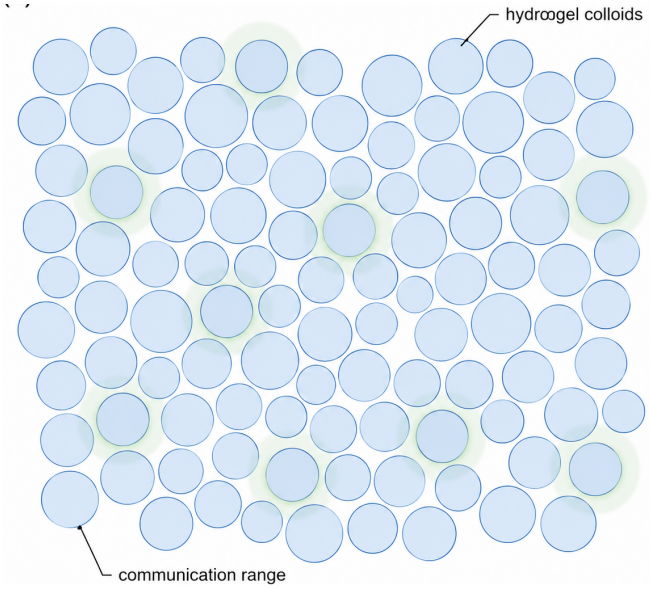

Figure 1. Representative two-dimensional monolayer of communicating hydrogel colloids. The disc size indicates the variable particle diameter, and the diffuse halos indicate the finite communication range used to construct the neighbour signal field.

The interpretive value of Figure 1 is that it shows why the monolayer cannot be classified by particle positions alone. A particle's influence extends beyond its physical disc through the communication halo, so a dilute-looking configuration may still be chemically coupled when halos overlap, whereas a crowded configuration may become mechanically mobile if shrinkage reduces disc size.

The elastic pair interaction is described by a repulsive Hertzian form,

$$\Phi_{ij}(r_{ij}, \sigma_i, \sigma_j) = \epsilon \left(1 - \frac{r_{ij}}{\sigma_{ij}}\right)^{5/2} \Theta\left(1 - \frac{r_{ij}}{\sigma_{ij}}\right), \qquad \sigma_{ij} = \frac{\sigma_i + \sigma_j}{2}, \tag{1}$$

The mechanical meaning of Eq. (1) is that overlap is tolerated but penalized with a nonlinear elastic cost. The force therefore becomes important only when instantaneous diameters and Brownian positions bring two soft colloids into contact. This is the point where chemical shrinkage can affect mechanics: by reducing σ_i, a particle lowers σ_{ij}, weakens contact, and opens free volume for rearrangement.

where $r_{ij} = |\mathbf{x}_j - \mathbf{x}_i|$, ϵ is the elastic interaction strength, and Θ is the Heaviside step function. Eq. (1) is not only an excluded-volume term. Because σ_i and σ_j are dynamic variables, the same expression converts chemical shrinkage

into free-volume release and chemical swelling into stronger mechanical contact. The pair potential therefore supplies the mechanical pathway through which a local chemical event can be transformed into a density rearrangement.

The isolated-particle size preference is represented by a finite-extensibility elastic potential,

$$U(\sigma_i) = -\frac{q\sigma_0^2}{8\beta} \ln\left[1 - 4\left(\frac{\sigma_i - \sigma_0}{\sigma_0}\right)^2\right], \tag{2}$$

Eq. (2) makes the isolated particle monostable rather than self-oscillatory. The logarithmic divergence restricts the admissible diameter window, while the near-centre curvature provides an elastic restoring tendency toward σ_0. Any sustained oscillation observed in the monolayer must therefore be attributed to communication and many-body feedback, not to a built-in bistable particle potential.

where σ_0 is the preferred diameter, q is the stiffness near σ_0, and $\beta = (k_B T)^{-1}$. The logarithmic divergence prevents physically excessive swelling or collapse and is essential for interpreting strong communication states. Without finite extensibility, a large chemical force could generate unrealistic size amplitudes and obscure the distinction between chemical response and elastic admissibility.

The total chemical field sensed by particle i is written as

$$S_i(t) = c_i(t) + \sum_{j \neq i} Y_{ji}(r_{ij}; c_j, \sigma_j), \tag{3}$$

Eq. (3) defines the sensed field as a genuinely collective quantity. A particle responds to its own concentration and to the chemically weighted presence of neighbours, so the relevant stimulus is not merely local production but the superposed communication environment. This is why the same particle can behave differently at the same c_i when placed in a dilute, semi-dilute, or crowded neighbourhood.

where the contribution of particle j has a Yukawa-type form,

$$Y_{ji}(r_{ij}; c_j, \sigma_j) = c_j \frac{\sigma_j}{2r_{ij}} \exp\left[-\kappa\left(r_{ij} - \frac{\sigma_j}{2}\right)\right]. \tag{4}$$

Eq. (4) converts neighbour identity into a distance-weighted chemical input. The exponential term gives the finite communication length, while the prefactor containing σ_j connects source strength to the size of the emitting hydrogel colloid. Larger or more productive neighbours therefore cast stronger chemical influence, but only over the range set by κ^{-1}.

The length κ^{-1} defines the range of communication. Equations (3) and (4) show that the received signal is strongest when the sender concentration is high, the sender diameter is large, and the separation is small. The exponential term restricts communication to a finite spatial range, whereas the $1/r_{ij}$ factor accounts for spatial dilution of a diffusive field.

Figure 2 gives the local pair interpretation of Eqs. (1)–(4). The same interparticle spacing controls the Hertzian contact contribution and the exponentially screened chemical signal; therefore, a local decrease in diameter simultaneously weakens mechanical overlap and modifies the intensity of chemical communication.

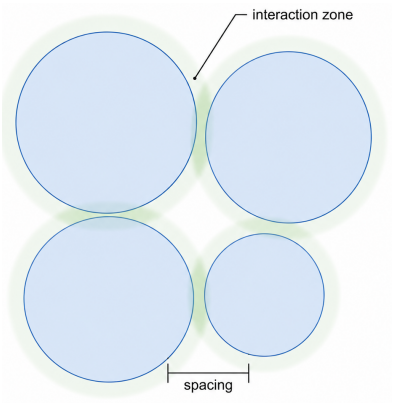

Figure 2. Pair-level interaction zone between size-responsive hydrogel colloids. The spacing between neighbouring particles controls both elastic contact and the overlap of their communication fields.

Figure 2 emphasizes that the pair relation contains two simultaneous channels. The centre-to-centre distance controls Hertzian contact when the soft cores overlap, while the same distance controls the exponential decay of chemical communication. Oscillation emerges only when these two channels are balanced rather than when either channel acts in

isolation.

The internal concentration follows a permeability-controlled production–loss relation,

$$\dot{c}_i = k_0 c_c \exp\left(-\frac{B}{\sigma_i^3}\right) - k_l c_i, \tag{5}$$

Eq. (5) introduces the delayed chemical part of the feedback loop. The production term increases with particle accessibility through its size dependence, whereas the loss term relaxes concentration over the characteristic chemical time. The competition between these terms determines whether a diameter change is followed by a persistent chemical signal or a rapidly extinguished fluctuation.

where k_0 is the production coefficient, c_c is a reference concentration, B is the sieving parameter, and k_l is the loss coefficient. The exponential dependence on σ_i^{-3} expresses the physical idea that a swollen hydrogel permits stronger fuel penetration and product generation, while a collapsed hydrogel suppresses conversion. This relation introduces a delay between size, permeability, concentration, and subsequent chemical signalling.

The overdamped size dynamics can be summarized as

$$\xi_\sigma \dot{\sigma}_i = \sum_{j\neq i} \frac{\partial \Phi_{ij}}{\partial \sigma_i} - \frac{\partial U}{\partial \sigma_i} - m\,[S_i(t) - c_c] + \eta_i^\sigma(t), \tag{6}$$

Eq. (6) is the central coupling relation of the material. Elastic contacts, single-particle restoration, chemical forcing, and thermal fluctuation all act on the same diameter variable. The sign of the chemical term means that a sensed field above c_c drives shrinkage, so collective communication can create a mechanical response even when no individual particle possesses an autonomous oscillatory cycle.

where ξ_σ is the size friction, m is the communication magnitude, and η_i^σ is the thermal size noise. A sensed field above c_c drives shrinkage, while a field below c_c allows swelling. This sign relation is the basis of the susceptibility method: the central observable is not only how large S_i becomes, but whether a high $S_i(t)$ predicts a later decrease of $\sigma_i(t+\Delta)$.

Table 1. Numerical and categorical quantities used for delay-resolved elastochemical susceptibility analysis. The table consolidates particle number, geometry, density, communication strength, elasticity, permeability, integration settings, and state-identification descriptors.

Quantity group	Value or range	Role in the susceptibility analysis
Particle number	$N = 1600$	Ensemble size for susceptibility and spectral averaging
Geometry	Two-dimensional periodic monolayer	Represents confined or sedimented responsive colloids
Density coordinate	$\rho\sigma_0^2 \approx 0.01$–$3.0$	Controls encounter rate, packing, and free-volume availability
Communication coordinate	$m/(q\sigma_0/c_c) \approx 0$–$20$	Controls chemical forcing of particle-size response
Communication length	$\kappa^{-1} = \sigma_0$	Sets finite range of Yukawa signal overlap
Elastic interaction strength	$\epsilon = 500\,k_\mathrm{B}\,T$	Prevents strong overlap and generates packing stress
Size stiffness	$q = 100\,k_\mathrm{B}\,T/\sigma_0^2$	Sets resistance to swelling and shrinkage
Size-friction coefficient	$\xi_\sigma = 10\xi_x^0$	Controls relaxation time of diameter fluctuations
Reference translational friction	$\xi_x^0 = 1\,k_\mathrm{B}\,T\tau/\sigma_0^2$	Defines the Brownian time scale τ
Production coefficient	$k_0 = 2.749/\tau$	Controls proton generation under permeable conditions
Loss coefficient	$k_l = 1/\tau$	Sets chemical relaxation time
Sieve parameter	$B = \sigma_0^3$	Couples hydrogel size to fuel permeability
Time step	$\Delta t = 10^{-4}\tau$	Integration resolution
Pre-measurement relaxation	5τ	Removes preparation effects
Measurement duration	40τ	Window for delayed correlations and spectral scores
Solid-state indicator	$\Psi_{18} > 0.5$	Identifies long-range hexagonal ordering
Cluster-wave indicator	Short-time superdiffusive wave response	Identifies propagating elastochemical clusters

Table 1 is important because it makes the analysis traceable from physical inputs to diagnostic outputs. The table separates prescribed material parameters, such as elasticity and signal length, from derived descriptors, such as susceptibility and packing occupancy. This separation prevents the classification from being treated as a fitted label and instead ties it to measurable or computable quantities.

For each particle, deviations from the time-averaged sensed field and diameter are defined as

$$\delta S_i(t) = S_i(t) - \langle S_i \rangle, \qquad \delta\sigma_i(t) = \sigma_i(t) - \langle \sigma_i \rangle, \tag{7}$$

The subtraction in Eq. (7) removes the stationary offset associated with density and average communication level. The analysis therefore focuses on dynamic departures from each particle's own mean state, which is essential when comparing dilute and crowded regimes with different average diameters.

where $\langle\cdot\rangle$ denotes averaging over the measurement window. The lagged signal–size susceptibility is then

$$\chi_{\sigma S}(\Delta) = \left\langle \frac{\langle \delta\sigma_i(t+\Delta)\delta S_i(t)\rangle_t}{\sqrt{\langle \delta\sigma_i^2\rangle_t \langle \delta S_i^2\rangle_t}} \right\rangle_i . \tag{8}$$

Eq. (8) is a normalized memory measure. Its value is insensitive to the absolute fluctuation amplitude and instead records the temporal order between signal and size. A negative minimum at finite Δ is the signature that chemical exposure is not merely simultaneous with size change but precedes shrinkage by a measurable delay.

A negative value of $\chi_{\sigma S}(\Delta)$ means that a high sensed chemical field is followed by a smaller particle diameter after lag Δ. The strongest delayed shrinkage response and its associated delay are defined as

$$\chi^{-}_{\sigma S} = -\min_{\Delta\in[0,2\tau]} \chi_{\sigma S}(\Delta), \qquad \Delta^{\star} = \arg\min_{\Delta\in[0,2\tau]} \chi_{\sigma S}(\Delta). \tag{9}$$

Eq. (9) reduces the lag curve to two physically interpretable numbers: the magnitude of the delayed shrinkage response and the delay at which it occurs. These values separate a noisy responsive liquid, where correlations remain weak, from a communication-activated material in which chemical events predict later mechanical deformation.

The amplitude $\chi^{-}_{\sigma S}$ measures the strength of communication-induced shrinkage, while $\Delta^{\star}$ measures the characteristic response time. This construction distinguishes true delayed chemical activation from instantaneous diameter anticorrelation produced by mechanical compression alone.

A representative normalized chemical-signal history is shown in Figure 3. The highlighted maximum marks the type of local chemical event used to evaluate whether a later diameter decrease occurs at the same particle. The important point is temporal ordering: the chemical exposure is read first, and the size response is tested at a positive delay.

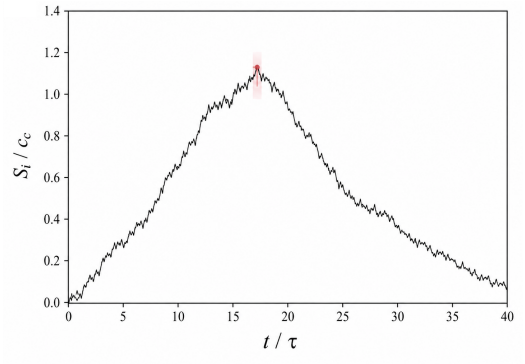

Figure 3. Representative local signal history S_i/c_c over the measurement window. The highlighted peak identifies a transient chemical exposure whose delayed effect on particle diameter is measured by the susceptibility $\chi_{\sigma S}(\Delta)$.

Figure 3 also clarifies why a lag-resolved measure is necessary. The important event is not only that the sensed signal rises, but that the following diameter trace responds after a finite interval. The peak therefore marks the beginning of a cause-and-response sequence that is lost in equal-time correlation analysis.

To account for finite communication range and density-dependent neighbour separation, the mean-distance communication number is introduced:

$$\Gamma(\rho, m) = \widehat{m}\frac{\sigma_0}{2\ell_\rho}\exp\left[-\kappa\left(\ell_\rho - \frac{\sigma_0}{2}\right)\right], \qquad \widehat{m} = \frac{m}{q\sigma_0/c_c}, \qquad \ell_\rho = \rho^{-1/2}. \tag{10}$$

Eq. (10) is a compact estimate of the communication actually experienced at the mean spacing. It shows why increasing $\widehat{m}$ and increasing density are not equivalent: the former strengthens the source response, whereas the latter changes the distance over which the Yukawa signal is attenuated. Their product determines whether neighbours are chemically visible to one another.

The parameter Γ increases when particles are closer, when communication is stronger, or when the decay length is comparable to the mean spacing. It therefore combines the two independent control variables into a physically interpretable estimate of neighbour influence.

The actual packing state is measured by the elastic occupancy

$$\Pi_e = \rho\bar{\sigma}^2, \tag{11}$$

Eq. (11) distinguishes nominal particle loading from elastic occupancy. Because $\bar{\sigma}$ is itself communication dependent, Π_e can decrease when chemical shrinkage is strong. The same number density may therefore correspond to a mechanically arrested solid or a shrinkage-fluidized active material.

where $\bar{\sigma}$ is the mean particle diameter. This differs from the nominal density $\rho\sigma_0^2$ because communication can reduce $\bar{\sigma}$. Thus, a system with high nominal density may remain mobile if chemical shrinkage lowers the effective occupied area.

The neighbourhood construction used for A_n is shown in Figure 4. Each particle is assigned a diameter, a local signal neighbourhood, and an ordered set of neighbouring particles; this makes it possible to test whether antiphase response is confined to the first coordination shell or persists across a wider local domain.

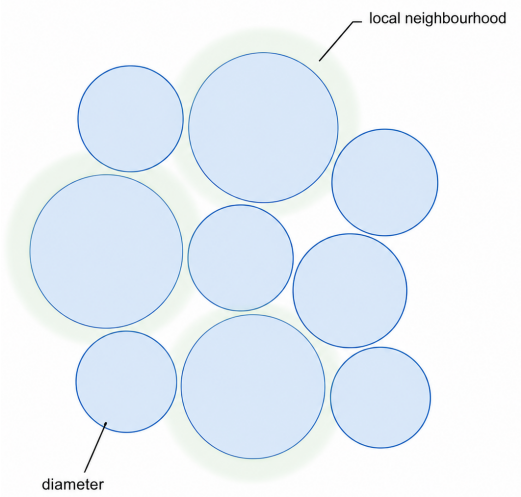

Figure 4. Local neighbourhood used for diameter tracking and neighbour-depth antiphase scoring. The labelled diameter defines the size degree of freedom, while the surrounding halo represents the communication neighbourhood sampled by nearby particles.

Figure 4 gives the spatial meaning of A_n. By increasing the number of neighbours included in the score, the analysis moves from pair alternation to shell-level organization. This distinction is important because a two-particle antiphase event does not by itself prove a collective material state.

The local antiphase score uses the n nearest neighbours of each particle:

$$A_n = -\left\langle \frac{1}{n} \sum_{j \in \mathcal{N}_n(i)} \frac{\langle \delta\sigma_i(t+\Delta^\star)\delta\sigma_j(t)\rangle_t}{\sqrt{\langle \delta\sigma_i^2\rangle_t \langle \delta\sigma_j^2\rangle_t}} \right\rangle_i . \tag{12}$$

Eq. (12) tests whether the delayed response is spatially organized. Positive A_n means that neighbours tend to occupy the complementary part of the size cycle, while its persistence with increasing n indicates that the alternation extends beyond a single pair into a coordinated local domain.

Large positive A_n indicates that neighbouring particles occupy opposite size phases after the characteristic response delay. In the present analysis, $n = 20$ is used as the principal local-neighbour scale, while $n = 6$, 12, and 36 provide a length-scale test of whether antiphase organization remains restricted to the nearest shell or extends over a broader local cluster.

Cluster-wave organization is detected by a spectral score. Let $\widetilde{S}(\mathbf{r}, t)$ be the normalized chemical signal field on a rectangular grid, and let $\widehat{S}(\mathbf{k}, \omega)$ denote its space-time transform. The propagating-wave score is

$$W_{\mathrm{cl}} = \frac{\max_{\mathbf{k}\neq 0,\ \omega>0} |\widehat{S}(\mathbf{k},\omega)|^2}{\sum_{\mathbf{k},\omega} |\widehat{S}(\mathbf{k},\omega)|^2}. \tag{13}$$

Eq. (13) prevents temporal oscillation from being confused with wave transport. A high value requires that a dominant portion of chemical-field power is concentrated at nonzero wave number and positive frequency, which is the spectral condition for a propagating cluster-wave mode.

A high W_{cl} requires the field to be organized at both finite frequency and finite wave number. It therefore separates a propagating cluster-wave state from local oscillation without spatial coherence or from static packing order without temporal propagation.

The workflow in Figure 5 makes the classification reproducible. It begins with measurable particle and chemical histories, derives time-lagged and packing-corrected descriptors, and only then assigns the state. This order reduces the

risk of assigning a regime from a visually striking snapshot without confirming the required temporal and mechanical evidence.

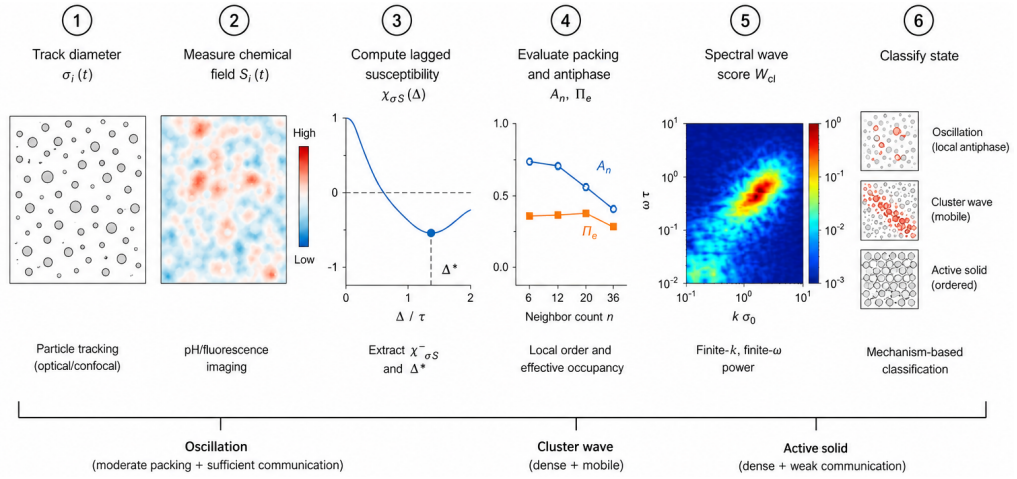

Figure 5. Analysis workflow for delay-resolved elastochemical state assignment. Particle diameters and chemical fields are first measured or computed, then converted into lagged susceptibility, packing, antiphase, and spectral descriptors before the material is classified as oscillatory, wave-like, or solid-like.

Figure 5 summarizes how the descriptors are combined. The workflow begins with particle tracking and chemical-field measurement, then extracts the delayed signal–diameter response, evaluates local occupancy and antiphase order, identifies finite-k and finite-ω wave content, and finally assigns the state using mechanism-based criteria rather than visual inspection alone.

Four numerical interrogations are defined. The first is a density–communication sweep in which $\rho\sigma_0^2$ is varied from dilute to compressed monolayer conditions and $\widehat{m} = m/(q\sigma_0/c_c)$ is varied from weak to strong communication. At each point, $\chi_{\sigma S}^{-}$, $\Delta^\star$, A_{20}, Π_e, and W_{cl} are evaluated. The second is a neighborhood-depth test in which A_n is computed for $n = 6, 12, 20$, and 36. A response confined to $n = 6$ indicates short-range alternation, whereas persistence to $n = 20$ or 36 indicates collective local organization. The third is a packing-corrected communication test comparing $\rho\sigma_0^2$ with Π_e, thereby separating chemical shrinkage from mechanical crowding. The fourth is a directed-disturbance test in which a concentration-skewed initial condition is used to determine whether a high-W_{cl} state supports transient oriented wave motion.

The state classification is summarized in Table 2. A state is assigned only when the susceptibility, antiphase, packing, and spectral indicators are consistent with the physical mechanism. This avoids assigning cluster-wave behaviour to a purely temporal oscillator or assigning antiphase order to a static packing artifact.

Table 2. State classification used in the delay-resolved elastochemical susceptibility method.

State	Diagnostic signature	Physical interpretation
Dilute active liquid	Low Γ, low A_{20}, low W_{cl}	Particles diffuse and communicate intermittently; chemical clouds rarely overlap long enough to create sustained delayed shrinkage.
Semi-dilute fluctuating liquid	Moderate Π_e, weak or moderate $\chi_{\sigma S}^{-}$	Elastic contacts occur, but chemical delay is not sufficiently organized to sustain a stable oscillatory pattern.
Delayed antiphase state	High $\chi_{\sigma S}^{-}$ and positive A_{20} at moderate Π_e	Neighbouring particles alternate between swollen and collapsed states through delayed mutual chemical stimulation.
Elastochemical cluster-wave state	High W_{cl}, high $\chi_{\sigma S}^{-}$, and Π_e near the crowded-fluid regime	Local shrinkage releases free volume; neighbours rearrange and swell into the released space, generating a propagating chemical-size-density pattern.
Active solid	$\Psi_{18} > 0.5$ and suppressed W_{cl}	Long-range hexagonal ordering dominates; communication modifies fluctuations but does not support liquid-like wave transport.

Table 2 turns the susceptibility analysis into explicit decision rules. A regime is accepted only when its temporal response, spatial organization, and mechanical state agree. This is necessary because any single descriptor can be ambiguous: a negative size correlation may arise from compression, a dense structure may be chemically inactive, and a spectral peak may be transient unless it is supported by the other diagnostics.

3 Results

The first result is that the onset of oscillatory communication is most clearly identified by a negative delayed susceptibility. In weakly coupled conditions, the sensed field $S_i(t)$ fluctuates because neighbours move into and out of communication range, but these fluctuations do not consistently predict later diameter changes. The susceptibility $\chi_{\sigma S}(\Delta)$ remains near zero over the lag interval, indicating that the particle behaves mainly as a Brownian responsive object with intermittent chemical exposure. In stronger communication conditions, an elevated $S_i(t)$ is followed by shrinkage, producing a negative minimum in $\chi_{\sigma S}(\Delta)$ and a finite response time $\Delta^\star$.

This distinction matters because instantaneous diameter correlations alone cannot identify the cause of a small particle. A particle may be small because it has sensed a high chemical field and is chemically activated, or because it is mechanically compressed by neighbours. Eq. (8) separates these possibilities by testing temporal order: chemical signal first, mechanical response second. The antiphase state is therefore not merely a region of negative size correlation; it is a region in which chemical sensing carries predictive information about subsequent shrinkage.

Figure 6 illustrates how the particle-scale fields fluctuate across the measurement window. The grey circle size reports the normalized particle diameter, while the red intensity reports c_i/c_c. The sequence shows that the relevant observable is not a single static configuration but the time-resolved co-evolution of diameter, concentration, and local packing.

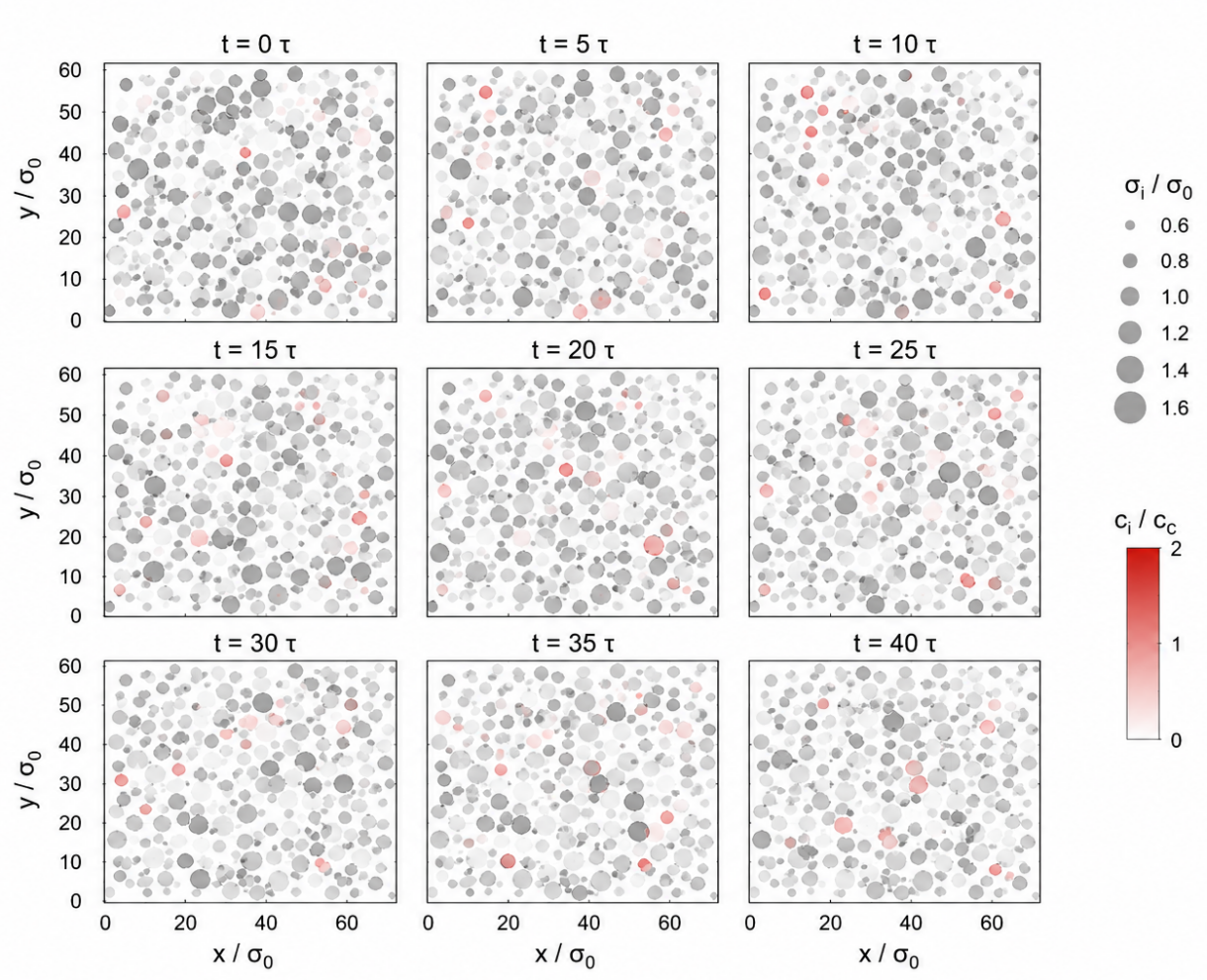

Figure 6. Time-resolved particle-size and concentration fields from $t = 0\tau$ to 40τ. Marker size represents σ_i/σ_0, and red intensity represents c_i/c_c, allowing local size response and chemical activity to be compared over the same interval.

Figure 6 provides the temporal bridge between equations and material behaviour. Local colour variation identifies the chemical field, while marker-size variation identifies the mechanical response. The figure therefore demonstrates that the relevant observable is the sequence of chemical enrichment, diameter change, and neighbourhood rearrangement, not any one field separately.

The density–communication map is more informative when the nominal density $\rho\sigma_0^2$ is read together with elastic occupancy Π_e. Nominal density describes how many reference-size particles occupy the monolayer, whereas Π_e describes how much area is actually occupied after communication-induced size change. Since strong communication promotes

shrinkage, increasing $\widehat{m}$ can lower $\bar{\sigma}$ and reduce the effective packing. The material may therefore remain dynamically rearrangeable at densities where a weakly communicating system would show solid-like ordering.

Table 3. Regime-level outcomes across the density and communication ranges resolved by susceptibility-based interpretation. Values are expressed as normalized regions rather than high-precision phase boundaries.

Control region	Dominant indicator	Mechanistic outcome
$\rho\sigma_0^2 \lesssim 0.02$	$\Gamma \ll 1$, weak $\chi_{\sigma S}^{-}$	Communication is too sparse for persistent collective oscillation; particles remain largely uncorrelated.
$\rho\sigma_0^2 \approx 0.1$–$0.5$ and $\widehat{m} \gtrsim 5$	Strong $\chi_{\sigma S}^{-}$ and positive A_{20}	Stable antiphase oscillation emerges through delayed mutual shrinkage and swelling.
$\rho\sigma_0^2 \gtrsim 1$ with high $\widehat{m}$	Rising W_{cl} and finite Π_e	Local oscillations organize into cluster-scale elastochemical waves.
$\rho\sigma_0^2 \gtrsim 2.4$ at low $\widehat{m}$	$\Psi_{18} > 0.5$, low W_{cl}	Hexagonal ordering dominates and suppresses liquid-like wave propagation.
High $\widehat{m}$ under dense conditions	Reduced $\bar{\sigma}$ and shifted Π_e	Chemical shrinkage lowers effective occupancy and moves solidification toward higher nominal density.

Table 3 summarizes the density–communication part of the analysis in practical terms. The regimes are expressed as normalized ranges rather than as sharp thermodynamic phase boundaries because the system is finite, fluctuating, and nonequilibrium. The table is therefore a design map: it indicates where one should tune density and communication to obtain local oscillation, cluster waves, or mechanically stabilized ordering.

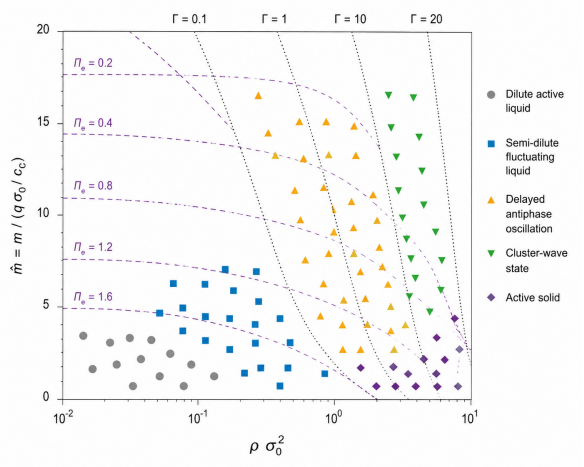

Figure 7. Density–communication state map for delay-resolved elastochemical interpretation. The horizontal axis is the normalized density $\rho\sigma_0^2$, and the vertical axis is the normalized communication coordinate $\widehat{m} = m/(q\sigma_0/c_c)$. Coloured symbols identify dilute active liquid, semi-dilute fluctuating liquid, delayed antiphase oscillation, cluster-wave state, and active solid regimes, while the dashed and dotted curves indicate effective occupancy and communication guides.

The state map in Figure 7 should be read as a mechanistic atlas rather than a purely empirical phase diagram. Moving upward increases communication forcing, moving rightward increases neighbour encounter frequency and crowding, and the regime boundaries indicate where the delay and packing conditions become mutually compatible with oscillation or wave propagation.

Figure 7 provides the resolved density–communication organization used to interpret the state map. The low-density corner remains a dilute active liquid because chemical encounters are too sparse. The intermediate-density and moderate-to-high-communication region supports delayed antiphase behaviour. The high-density and high-communication region supports cluster-wave propagation because delayed shrinkage and elastic crowding cooperate. The high-density and low-communication region forms an active solid because insufficient shrinkage leaves the packing mechanically constrained. The figure also clarifies why communication can both increase activity and postpone solidification: it strengthens the chemical driving force while lowering the effective occupied area.

The antiphase state can be understood as a distributed delay cycle shared by neighbouring particles. A swollen particle has increased permeability and can maintain or generate a stronger internal product concentration. This enhances the field sensed by nearby particles. A neighbour that senses the elevated field subsequently shrinks because the chemical term in Eq. (6) opposes swelling when $S_i(t) > c_c$. After shrinkage, production is reduced by Eq. (5), the local field relaxes, and the particle becomes able to swell again. The neighbouring particle may then enter the complementary part of the cycle, creating an alternating size pattern.

The physical meaning of A_n is therefore more specific than a pair correlation coefficient. It measures whether the alternating response persists over a selected neighbourhood after the susceptibility-defined delay $\Delta^\star$. If A_6 is high but A_{20} is weak, the state is a nearest-neighbour alternation without broader local organization. If A_{20} remains high, several shells participate in the delay cycle. If A_{36} remains high, the oscillation approaches cluster-scale organization and may become a precursor to wave formation.

The neighbour-depth dependence of the antiphase score is shown in Figure 8. The weak-communication curve remains near zero because neighbours do not maintain a reproducible delayed alternation. The delayed-antiphase and cluster-wave curves remain positive over increasing n, indicating that the oscillatory response extends beyond immediate pairs and becomes a collective local material property.

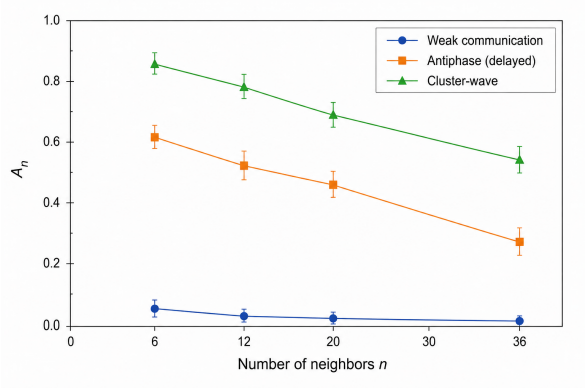

Figure 8. Neighbour-depth antiphase score A_n for weak communication, delayed antiphase oscillation, and cluster-wave conditions. Persistence of positive A_n over larger neighbour counts indicates that antiphase organization extends across multiple local coordination shells.

Figure 8 distinguishes local alternation from extended collective order. A strong score at small neighbour number indicates pair-level antiphase response, whereas persistence at larger neighbour depth shows that the delay cycle has spread through a wider region of the material. This is the difference between a transient local event and a genuine collective oscillatory state.

Cluster waves occur when delayed chemical response is embedded in a dense but mobile packing. In such a state, a group of particles that experiences a high chemical signal begins to shrink. Shrinkage decreases local excluded area and releases free volume. Neighbouring particles then move into the released space and may swell as their local chemical field changes. This creates a coupled modulation of concentration, diameter, and density. The wave is therefore not a chemical wave alone and not an elastic wave alone; it is an elastochemical release-and-refill process.

A directed cluster-wave evolution is shown in Figure 9. As the red concentration-rich domain develops, the active cluster shifts through the colloid field rather than remaining as a stationary fluctuation. The snapshots therefore provide the real-space counterpart to the spectral requirement that cluster waves possess both spatial and temporal organization.

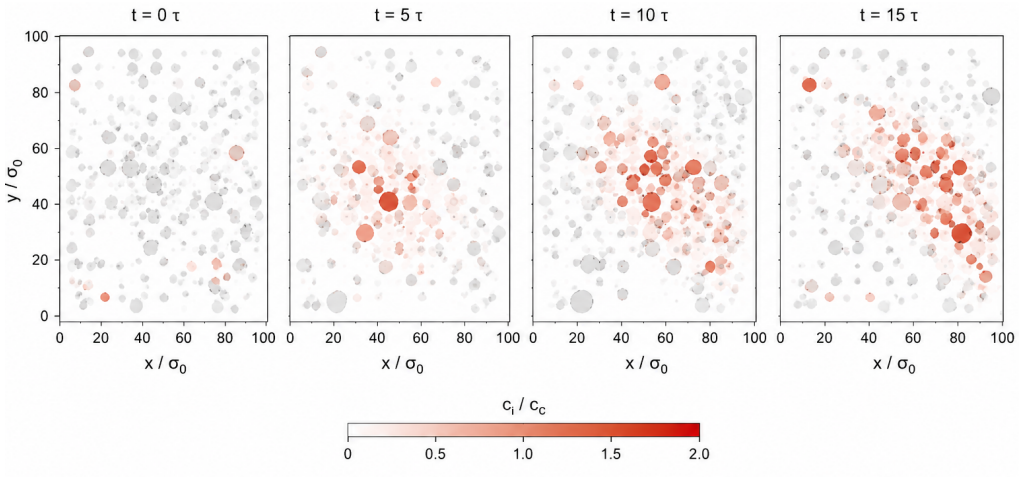

Figure 9. Real-space evolution of a cluster-wave event from $t = 0\tau$ to 15τ. Red intensity denotes the normalized concentration c_i/c_c, while marker size tracks the responsive colloid diameter, showing the coupled movement of chemical enrichment and size modulation.

The cluster-wave sequence in Figure 9 is best interpreted as a moving zone of chemical-mechanical conversion. Concentration enrichment initiates shrinkage, shrinkage releases area, and neighbouring particles refill the released volume. The propagating feature is therefore a coupled modulation of chemistry, diameter, and density rather than a passive concentration front.

The spectral score W_{cl} was introduced to detect this coupled organization. A purely local oscillator can show strong temporal periodicity without a finite wave-number peak. A crowded but chemically weak packing can show spatial order without finite-frequency propagation. A cluster wave requires both: chemical-size fluctuations must be organized spatially and temporally. A high W_{cl} therefore identifies a state in which localized delay cycles have synchronized into a propagating pattern.

The distinction between local oscillation, static solid-like order, and cluster-wave propagation is reinforced by the combined real-space and spectral signatures in Figure 10. A local oscillator is dominated by temporal response with weak finite-wavelength organization, a static or solid-like state shows a strong structural signature without propagating chemical-wave content, and the cluster-wave state produces a compact finite-k, finite-ω intensity maximum.

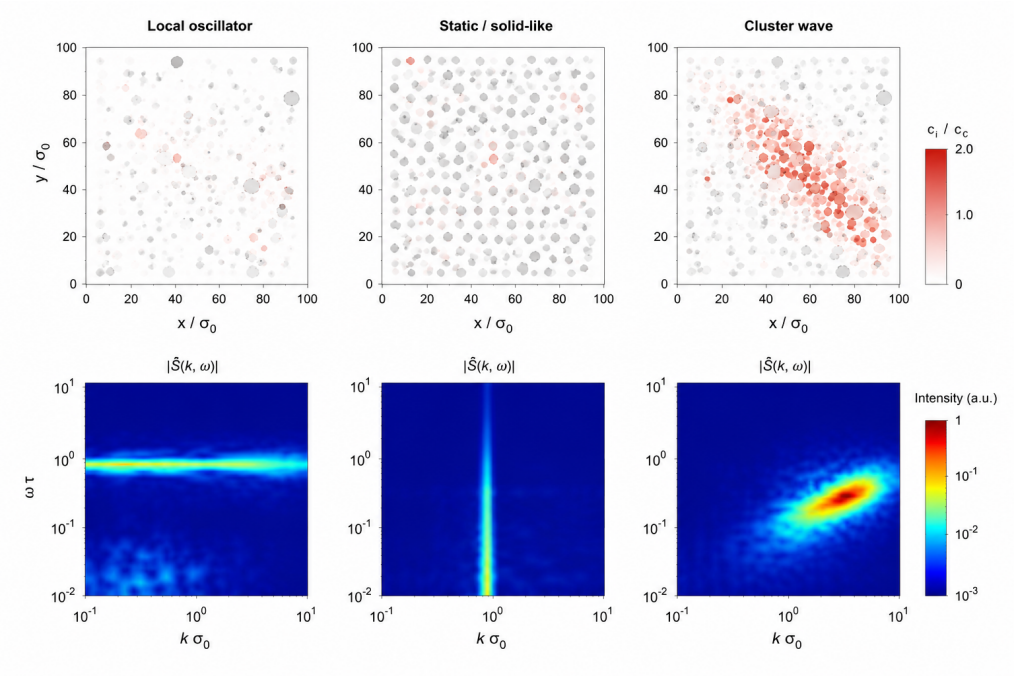

Figure 10. Real-space configurations and spectral signatures for local oscillator, static/solid-like, and cluster-wave regimes. The lower panels show $|\hat{S}(k,\omega)|$, where a finite wave-number and finite-frequency intensity maximum identifies propagating cluster-wave organization.

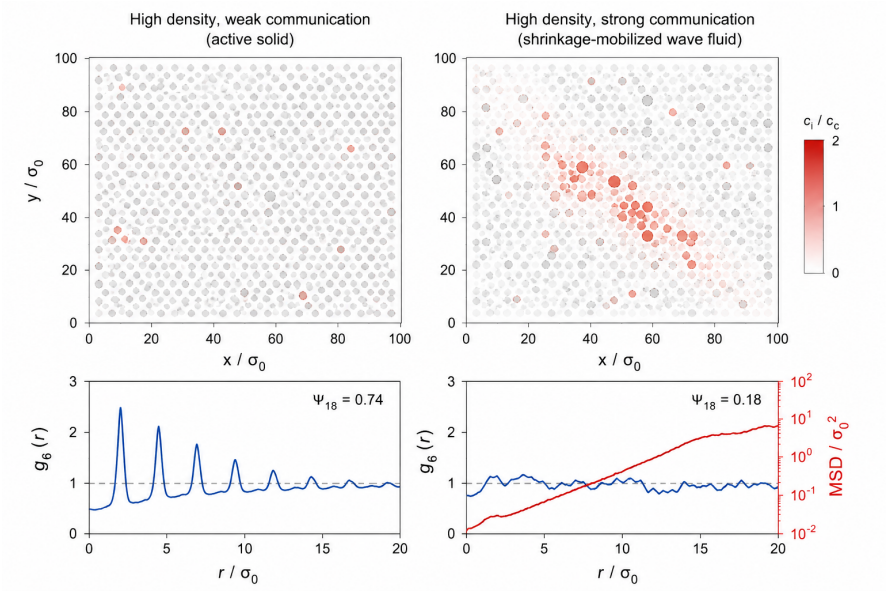

Figure 11. Comparison of dense weak-communication and dense strong-communication states. The weak-communication system behaves as an active solid with high hexatic order, while the strong-communication system becomes a shrinkage-mobilized wave fluid with lower Ψ_{18} and increasing mean-squared displacement.

Figure 10 supplies the frequency-domain validation of the visual wave assignment. Local oscillators lack a dominant finite-k propagating signature, while solid-like states can display structural order without temporal transport. The cluster-wave regime is identified by the simultaneous presence of spatial and temporal concentration-field organization.

Figure 11 compares the high-density solid-like regime with a high-density strongly communicating wave-fluid regime. The weak-communication state retains positional order, expressed by pronounced peaks in $g_6(r)$ and a large hexatic order parameter. Strong communication lowers the effective order and increases the mean-squared displacement, indicating that chemical shrinkage restores mobility and permits wave transport.

Figure 11 explains why high density does not have a single outcome. At weak communication, dense packing favours solid-like order and limited rearrangement. At strong communication, shrinkage reduces effective occupancy and permits mobility, allowing the dense material to behave as a wave-supporting active fluid.

4 Discussion

The communication number $\Gamma(\rho, m)$ reveals the reason for the non-monotonic relationship between density/coupling and antiphase oscillation. At very small density, $\ell_\rho = \rho^{-1/2}$ is large, and the Yukawa signal from nearby particles decays rapidly. Even with a finite communication magnitude, the effective signal from neighbours is weak. With moderate density, particles are close enough for their signals to overlap during the chemical response lag, allowing for closure of the delay cycle. With high density, many neighbours can contribute at once, reducing the effect of the alternating pairing and initiating a transition to cluster-scale fluctuation.

The key conclusion is that communication enables a temporal balance among several mechanisms. The communication period must be sufficiently long for the received signal to change the size of the responding particle. The local particle arrangement must also be sufficiently dynamic to allow the alternative of swelling and shrinking. If the Brownian rearrangement of the neighbours is faster than the chemical response, the signal-response link will become disconnected. On the other hand, if the local arrangement of contacts is static, then the size fluctuation cannot respond dynamically to the signal and becomes constrained by the elastic network. The maximum communication effectiveness, defined as the maximal negative susceptibility, thus requires that the three effects coincide.

Another outcome is the role of the critical communication delay for collective phase propagation. When $\Delta^\star$ is significantly shorter than the local neighbour residence time, the shrinking happens before the neighbour loses significance in terms of chemical activity and the organization of antiphase pairs can be strengthened. Otherwise, when $\Delta^\star$ is significantly larger than the local neighbour residence time, the size response occurs after the local environment had already changed and the spatial coherence of antiphase dynamics is lost. The appearance of the oscillatory behaviour thus is a time-scale matching problem: loss rate, size relaxation, particle contact duration and communication length should be balanced in the same temporal window.

Table 3 confirms that communication plays dual roles here. Communication serves as the source of the chemical field, as the larger magnitude induces a stronger delayed size change. Communication is also a determinant of packing, since the shrinkage releases extra volume and affects elastic occupancy. Both of these processes cannot be treated independently. Communication at higher magnitudes will enhance the oscillatory regime while inhibiting solidification, since particles will be more shrunken and will not form elastic networks. Alternatively, weak communication will facilitate elastic ordering in the case of high density, as particles retain their enlarged sizes.

Such an interpretation provides additional insight into the phase map. The dilute region cannot simply be regarded as “low density” since the chemical field received from the neighbours is not strong and sustained enough to induce the delayed response. Antiphase region is not “moderate communication”, but the region where signal and response timescales match each other. The cluster wave region is not “high density”, but rather the crowded state which is still mobile enough to allow free-volume generation. Finally, the active solid is not a completely ordered crystalline material; however, it suppresses the liquid-like behaviour needed to sustain cluster waves due to positional order at large distances.

The packing correction provides additional explanation of why higher communication magnitude has contradictory effects. Increasing the signal magnitude not only amplifies chemical forcing, but also shrinks particles, effectively softening the packing interactions. Therefore, with the increasing $\widehat{m}$, the material can experience both organization of oscillatory regime and mobility restoration, depending on the actual value of Π_e. Hence, the impact of communication on the material properties is not monotonic. Higher signaling ability can either lead to antiphase oscillations or induce fluid behavior in a packed state.

The suggested framework also demonstrates why oscillation is not inevitable in a monostable particle. Both elasticity potential and the production-loss equation describe the particle response that tends to converge to the equilibrium steady-state solution. To generate oscillatory regimes, communication needs to provide additional feedback that introduces a delay element in chemical response. Thus, the oscillator is no longer a property of a single colloid; it is an emergent phenomenon arising from the interaction of communicating particles. It is worth noting the applicability of the insight in designing novel materials with programmable oscillatory regimes.

The idea behind antiphase oscillations implies a specific temporal order of events, i.e., the sequence of chemical enrichment followed by size shrinking and finally the opposite process experienced by the adjacent particle. The directionality

of the delay process allows drawing mechanistic conclusions about the propagation of phase in the neighbour shells.

The propagation of cluster wave regime is assisted by the dual effect of communication. The enhanced magnitude produces stronger delayed shrinkage, leading to better volume release. At the same time, shrinkage lowers the value of Π_e, maintaining the mobility of a high-density material. Consequently, wave formation is expected in the vicinity of the dense but active regime, whereas dense rigid state and dilute regions are not suitable for wave propagation. In dilute conditions, the amount of neighbours is too low to induce a coordinated release of free volume. In a solid-like state, contacts become stable, making wave propagation inefficient. Cluster waves occur in the intermediate dense-active regime.

As mentioned above, cluster wave regime places the highest requirements on the materials studied. The local delayed response, the appropriate level of neighbour connectivity and a certain degree of particle mobility are necessary. Any two of these conditions might be satisfied individually, making the spectral approach the final confirmatory step.

The analysis provides some insights on the design of the system under study. For localized oscillation, the communication length scale should be comparable to the mean separation distance between particles and the signal magnitude needs to produce finite negative susceptibility, but without inducing excessively dense state. Under such conditions, the positive and robust A_{20} indicates the participation of the neighbourhood in oscillations.

Cluster-wave propagation requires higher density to create elastic contacts that will enable release of free volume. At the same time, this state needs to stay below the threshold of high Π_e that suppresses rearrangement. This effect can be achieved by choosing the appropriate communication magnitude, capable of promoting shrinking and retaining low values of Π_e. Thus, shrinkage turns out to be a multi-purpose phenomenon – not only a simple chemical response but also a mechanical control factor that maintains the mobility of the material.

For directional wave propagation, a spatially asymmetric system should be employed. While a perfectly regular arrangement of particles can give rise to wave dynamics with different directions of propagation, a gradient of particle density, patterned fuel delivery or local illumination creates preferred wave orientation. Such a feature could allow for designing materials with controlled transient transport, triggered by the chemical patterning without requiring any actuation.

The approach itself is experimentally feasible. Tracking particle sizes using microscopy and estimating chemical signal via fluorophore concentration or other observable fields can give clear indications of whether communication leads to antiphase oscillation. Combining these measurements with the calculation of Π_e and spectral analysis of chemical signal will make it possible to differentiate antiphase oscillation, cluster wave and mechanically induced anticorrelated phases.

In summary, a set of time scales determines whether communication will result in oscillatory or stationary phenomena. In particular, the combination of chemical forcing, delayed signal-response, mechanical occupancy and elastic mobility needs to have proper scaling properties to allow for collective phenomena. The proposed scheme for determining communication-induced oscillation gives the following steps: measuring the local chemical signal and particle diameters, detecting the delay of the latter with respect to the former, verifying neighbour-based oscillation using spectral decomposition of chemical fields. Only this procedure will allow discriminating antiphase oscillation from mere size fluctuations or mechanical anticorrelations.

5 Conclusions and Outlook

In this way, the current research answers its main scientific question: collective oscillation in responsive hydrogel colloids is only possible when all of chemical communication, delay of the size response, neighbour residence times, and elastochemical release conditions are concurrently suitable. Chemical communication level per se cannot predict the oscillation occurrence. High communication number increases the intensity of the detected field; however, oscillation will appear only if the resulting field leads to the mechanical response with a time lag and if the local particle packing is still able to respond by rearrangement of its constituents. Thus, delay-dependent elastochemical susceptibility provides the missing mechanism between the map of the state and a particular realization of it.

As the main characteristic, $\chi_{\sigma S}(\Delta)$ shows the probability that a particle having increased the chemical field at time t will decrease its diameter shortly after, at $t+\Delta$. Its minimum, $\chi^{-}_{\sigma S}$, and corresponding delay, $\Delta^{\star}$, are a good measure of communication-induced activity. Then, the packing-compensated communication number Γ describes whether a neighbour is chemically perceptible at the mean inter-particle distance. Elastochemical occupancy Π_e tells if a certain density is actually acting like an elastic obstacle for neighbours. The neighbourhood score A_n describes how well the antiphase condition of delayed oscillations can be fulfilled locally or globally, whereas the spectral score W_{cl} allows checking if a periodic pattern of finite frequency and finite wavelength is observable within the communication region. Altogether, these characteristics distinguish dilute responsive liquids, semi-dilute liquids with chemical fluctuations, delayed antiphase oscillatory regimes, cluster waves, and elastochemically stabilised dense active solids.

The new interpretation of the presented results enables proposing a clear physical interpretation of them. In the antiphase region, a particle is capable of creating a larger field of chemical substance; the other particle feels the field and shrinks some time afterwards; and the first particle proceeds into the opposite phase of the process cycle. Thus, the oscillator exists distributed through the communicating particle ensemble rather than being enclosed inside a particle. In the cluster wave regime, this local delayed oscillatory cycle is embedded into a dense packing that is still rearrangeable.

Shrinkage releases free volume around particles; particles occupying the released volume again; and this coupling between concentration, size, and density modulations occurs as a wave event. By contrast, in the active solid regime, despite the presence of chemical signal variations, high elastochemical occupancy prevents the necessary rearrangement of particles, and thus, the wave dynamics is not possible here.

These findings have several implications concerning material design. To obtain antiphase oscillatory behaviour, it is required to reach moderate density, finite communication range, and an appropriate delay. However, for achieving cluster wave dynamics, a more dense packing should be provided, which cannot be too ordered so as not to hinder the rearrangement. On the one hand, strong communication may help wave propagation via increasing shrinking responses; on the other hand, it reduces the elastochemical occupancy, which helps the waves propagate. Consequently, experimental control over the particle rigidity, permeability, production rate, signal lifetime, and monolayer density would enable choosing between localized oscillation and propagative elastochemical dynamics.

Finally, it has become obvious which experimental observations can confirm or reject the obtained theoretical results. Particle positions and their sizes must be recorded by means of optical microscopy or confocal laser scanning. Particle pH or the level of a certain compound can be estimated via corresponding fluorescence. Negative delayed correlations between chemical signals and particle size will be the clearest proof of chemical communication triggering shrinking response. Moreover, combining it with measurements of occupancy, neighbourhood depth anticorrelations, and signal spectroscopy will allow experimentally distinguishing responsive liquids, antiphase oscillatory clusters, cluster waves, and dense mechanically stable states. Therefore, the conclusion is that chemical communication affects soft matter; nevertheless, the proposed research question is answered by this very particular effect.

References

[1] C. M. Waters and B. L. Bassler, "Quorum sensing: cell-to-cell communication in bacteria," *Annual Review of Cell and Developmental Biology*, vol. 21, pp. 319–346, 2005.

[2] T. Danino, O. Mondragón-Palomino, L. Tsimring, and J. Hasty, "A synchronized quorum of genetic clocks," *Nature*, vol. 463, pp. 326–330, 2010.

[3] C.-P. Heisenberg and Y. Bellaïche, "Forces in tissue morphogenesis and patterning," *Cell*, vol. 153, pp. 948–962, 2013.

[4] A. P. Dhanarajan, G. P. Misra, and R. A. Siegel, "Autonomous chemomechanical oscillations in a hydrogel/enzyme system driven by glucose," *Journal of Physical Chemistry A*, vol. 106, pp. 8835–8838, 2002.

[5] V. V. Yashin, O. Kuksenok, P. Dayal, and A. C. Balazs, "Mechano-chemical oscillations and waves in reactive gels," *Reports on Progress in Physics*, vol. 75, article 066601, 2012.

[6] D. J. Bell, D. Felder, W. G. von Westarp, and M. Wessling, "Towards synergistic oscillations in enzymatically active hydrogel spheres," *Soft Matter*, vol. 17, pp. 592–599, 2021.

[7] B. Blanc, J. N. Agyapong, I. Hunter, J.-C. Galas, A. Fernandez-Nieves, and S. Fraden, "Collective chemomechanical oscillations in active hydrogels," *Proceedings of the National Academy of Sciences of the United States of America*, vol. 121, article e2313258121, 2024.

[8] S. Saha, R. Golestanian, and S. Ramaswamy, "Clusters, asters, and collective oscillations in chemotactic colloids," *Physical Review E*, vol. 89, article 062316, 2014.

[9] J. Agudo-Canalejo and R. Golestanian, "Active phase separation in mixtures of chemically interacting particles," *Physical Review Letters*, vol. 123, article 018101, 2019.

[10] B. Liebchen and H. Löwen, "Chemical kinetics of active colloids," in *Chemical Kinetics: Beyond the Textbook*, World Scientific, pp. 493–516, 2019.

[11] J. Ventura, A. Llopis-Lorente, L. K. E. A. Abdelmohsen, J. C. M. van Hest, and R. Martínez-Máñez, "Models of chemical communication for micro/nanoparticles," *Accounts of Chemical Research*, vol. 57, pp. 815–830, 2024.

[12] S. Milster, A. Darwish, N. Göth, and J. Dzubiella, "Synergistic chemomechanical dynamics of feedback-controlled microreactors," *Physical Review E*, vol. 108, article L042601, 2023.

[13] N. Göth and J. Dzubiella, "Collective chemo-mechanical oscillations and cluster waves in communicating colloids," *Communications Physics*, vol. 8, article 65, 2025.